Biomedicine & Pharmacotherapy 142 (2021) 111968

Contents lists available at ScienceDirect

Biomedicine & Pharmacotherapy

journal homepage: www.elsevier.com/locate/biopha

Increased P2×2 receptors induced by amyloid-β peptide participates in the neurotoxicity in alzheimer's disease

Pamela A. Godoy [a,1], Daniela Mennickent [a,1], Inmaculada Cuchillo-Ibáñez [b,c], Oscar Ramírez-Molina [a], Tiare Silva-Grecchi [a], Jessica Panes-Fernández [a], Patricio Castro [d], Javier Sáez-Valero [b,c], Jorge Fuentealba [a,e,*]

[a] Laboratorio de Screening de Compuestos Neuroactivos, Departamento de Fisiología, Facultad de Ciencias Biológicas, Universidad de Concepción, Concepción, Chile
[b] Instituto de Neurociencias de Alicante, Universidad Miguel Hernández-CSIC, Sant Joan d'Alacant, 03550 Alicante, Spain
[c] Centro de Investigación Biomédica en Red sobre Enfermedades Neurodegenerativas (CIBERNED), Spain
[d] Departamento de Fisiología, Facultad de Ciencias Biológicas, Universidad de Concepción, Concepción, Chile
[e] Centro de Investigaciones Avanzadas en Biomedicina (CIAB-UdeC), Universidad de Concepción, Concepción, Chile

ARTICLE INFO

Keywords:
P2×2
Purinergic receptors
Amyloid beta
Alzheimer's disease
Fe65
APP

ABSTRACT

Amyloid beta peptide (Aβ) is tightly associated with the physiopathology of Alzheimer's Disease (AD) as one of the most important factors in the evolution of the pathology. In this context, we previously reported that Aβ increases the expression of ionotropic purinergic receptor 2 (P2×2R). However, its role on the cellular and molecular Aβ toxicity is unknown, especially in human brain of AD patients. Using cellular and molecular approaches in hippocampal neurons, PC12 cells, and human brain samples of patients with AD, we evaluated the participation of P2×2R in the physiopathology of AD. Here, we reported that Aβ oligomers (Aβo) increased P2×2 levels in mice hippocampal neurons, and that this receptor increases at late Braak stages of AD patients. Aβo also increases the colocalization of APP with Rab5, an early endosomes marker, and decreased the nuclear/cytoplasmic ratio of Fe65 and PGC-1α immunoreactivity. The overexpression in PC12 cells of P2×2a, but not P2×2b, replicated these changes in Fe65 and PGC-1α; however, both overexpressed isoforms increased levels of Aβ. Taken together, these data suggest that P2×2 is upregulated in AD and it could be a key potentiator of the physiopathology of Aβ. Our results point to a possible participation in a toxic cycle that increases Aβ production, Ca^{2+} overload, and a decrease of PGC-1α. These novel findings put the P2×2R as a key novel pharmacological target to develop new therapeutic strategies to treat Alzheimer's Disease.

1. Introduction

AD is characterized by two histopathological markers: neurofibrillary tangles and amyloid plaques [1], that are insoluble aggregates of amyloid-β peptide (Aβ). Dysregulation of APP processing and the subsequent increment in the Aβ levels are the key steps in AD pathogenesis [2]. Several evidence have proposed that soluble oligomer of Aβ (Aβo) are the main toxic species in AD that eventually lead to synaptic failure [3–8]. Aβ peptide is produced by the amyloidogenic cleavage of APP, this protein can also be proteolytically processed in the non-amyloidogenic pathway [9,10]. It has been described that these different processing pathways of APP occur in separate cellular compartments. The non-amyloidogenic processing mostly in the plasma membrane [11], while the amyloidogenic pathway takes place in

Abbreviations: AD, Alzheimer's disease; Aβ, Amyloid beta; Aβo, Oligomers of Aβ; AICD, Amyloid intracellular domain; APP, Amyloid precursor protein; ATP, Adenosine triphosphate; BDNF, Brain-derived neurotrophic factor; GSK-3β, Glycogen synthase kinase 3 beta; LRP1, Low-density lipoprotein receptor-related protein 1; LRP1b, Low-density lipoprotein receptor-related protein 1b; NMDA, N-methyl-D-aspartate; P2XR, Purinergic ionotropic receptor P2X; PPADS, Pyridoxalphosphate-6-azophenyl-2′,4′-disulfonic acid; RME-6, Receptor-mediated endocytosis 6; sAPPα, Amyloid precursor protein soluble alpha; sAPPβ, Amyloid precursor protein soluble beta.

* Correspondence to: Laboratorio de Screening de Compuestos Neuroactivos, Facultad de Ciencias Biológicas, Departamento de Fisiología, Universidad de Concepción, PO Box 160-C, Barrio Universitario s/n, Concepción, Chile.
E-mail address: jorgefuentealba@udec.cl (J. Fuentealba).
[1] PA Godoy and D Mennickent should be considered joint first authors.

https://doi.org/10.1016/j.biopha.2021.111968
Received 13 April 2021; Received in revised form 20 July 2021; Accepted 23 July 2021
Available online 31 July 2021

intracellular compartments, mainly in endosomes [9,12]. This endocytosis of APP makes represent a key step in the production of the Aβ peptide [12,13].

It has been postulated that Aβo perforate plasma membranes [5,14], allowing the passage of small molecules and metabolites such as ATP, according to the concentration gradient [7,15]. This helps to explain some of the events described in models of AD that correlate with physiopathology features of the disease. I.e. Ca^{2+} dyshomeostasis, ATP leakage, mitochondrial dysfunction and synaptic failure [15–19]. The increment in extracellular ATP induces a paracrine or autocrine activation of purinergic ionotropic receptors P2X (P2XR) in the vicinity. The 7 different subunits form trimeric cation permeable channels and act as neuromodulators of synaptic activity, inducing a facilitation of neurotransmitter release in neuronal and glial cells [20–22]. Some of these receptors are implicated in AD and other neurodegenerative diseases [23]. One of the toxic features observed in AD is chronic neuroinflammation [24], and the participation of P2×7R and P2×4R expressed in microglia has been observed [25]. Our group has shown the participation of P2XR in some of the toxic features induced by Aβo. One of this is the increment in intracellular Ca^{2+} levels, that could be partially prevented by using PPADS, a P2XR antagonist [7], this suggests an increased P2X activation-ATP dependent. Then, we have described an increment in P2×2R in different cell cultures related to the chronic Aβo treatment [26]. P2×2R is one of the most widely distributed subtype of P2XR. It is abundantly expressed in the periphery and central nervious systems, a slow desensitization and high sensitivity to ATP (low half maximal effective concentration, EC_{50}) [27]. The presence of P2×2R is observed in axons and close to nerve terminals, where they participate in the regulation of neurotransmitter release in hippocampal interneurons [21]. One of the most important properties of these receptores is related to a relatively high calcium permeabilty [28], that could be important to maintain the cytosolic Ca^{2+} homeostasis. The two main isoforms are P2×2a and P2×2b. P2×2a contains the complete exonic sequence, and P2×2b lacks 69 amino acids in the C terminus region [29]. This portion could be important to some relevant interaction with key intracellular factors, for example the interaction of P2×2a with Fe65 [29], an adaptor protein that can also interact with APP. The evidence shows that this interaction regulates APP endocytosis, and could regulate APP processing and Aβ generation [30].

Although P2×2R overexpression has been reported after treatment with Aβo, it is unclear the possible impact on the mechanisms of Aβo toxicity. Furthermore, no previous study has investigated the P2×2 expression on brain from patients with AD. In our present work, we explored the possible toxic effects of P2×2R overexpression and the crosstalk with Aβo. We evaluated the impact on some key intracellular proteins and mechanisms such as Fe65, APP endocytosis and Aβ generation, events that can induce a neuronal death and synaptic dysfunction. Furthermore, the finding of an altered presence of the receptor in the cortex of AD patient samples support our hypothesis that P2×2R is involved in the pathophysiology of AD. Together, these data represent a significant advance toward a comprehensive mechanism of Aβo toxicity and the participation of P2×2R in AD.

2. Materials and methods

2.1. PC12 cell culture

PC12 cells were obtained from ATCC (Cat# CRL-1721, RRID: CVCL_0481, Manassas, VA, USA) and were cultured as described by Gavilan et al., [31]. Briefly, they were maintained in DMEM (Corning, NY, USA) supplemented with FBS (5%) (Gibco, Grand Island, NY, USA), HS (5%) (Gibco, Grand Island, NY, USA), and penicillin-streptomycin (1%) (Gibco, Grand Island, NY, USA). Cells were incubated under standard conditions (37ºC, 5% CO_2). When 70–80% confluence was achieved, the cells were treated or transfected with P2×2a (1 μg), P2×2b (1 μg) and/or mCherry (0.5 μg) coding plasmids using Lipofectamine-2000 (Invitrogen, CA, USA). Cultures were used 24 h after transfection.

2.2. Mice primary hippocampal culture

Pregnant C57BL/6 mice were treated in accordance with the regulations recommended by NIH and the Ethics Committee of the Universidad de Concepción (Concepción, Chile) complying with the current laws in Chile. Primary cultures of embryonic hippocampi (E18) were obtained as described in Gavilan et al., [31]. Briefly, cells were plated at 320,000 cells/ml on coverslips coated with poly-L-lysine (Trevigen, Gaithersburg, MD, USA) in MEM (Gibco, Grand Island, NY, USA) supplemented with 10% HS, 4 mg/ml DNAse and 2 mM L-glutamine (Gibco, Grand Island, NY, USA) for 24 h. Culture medium was replaced after 24 h with MEM, 2% HS, 2% FBS and 0.5% N_3 (BSA 1 mg/ml, putrescine 4 mg/ml, insulin 1.25 mg/ml, sodium selenite 1 μg/ml, TH3 2 μg/ml, progesterone 1.25 μg/ml, corticosterone 4 μg/ml). The cell cultures were maintained at 37ºC with 5% CO_2. Experiments were performed at 10–11 DIV in control and treated neurons.

2.3. J20 hippocampal slices

Brain slices were obtained from J20 transgenic mice, a C57BL/6 J mice with human mutated APP KM670/671NL (Swedish) and V717F (Indiana), and C57BL WT mice. Animals were manipulated in accordance with the ethical regulations established by NIH and University of Concepción, and under the 3B criteria, one mouse from each phenotype was used to obtained the brain slices. Intracardiac perfusion was performed after 24 h of liquid diet and under Ketamine/Xylazine anesthesia. First, a perfusión with saline solution was performed (NaCl 0,9%). Next, a fixing solution (paraformaldehyde 4%) was used. The brains were extracted and post-fixed in the same solution (4 h, 4 °C). Lastly, the brains were in etanol (24 h, 4 °C) and brain slices of 60 μM were obtained in a vibratome Leica VT10005.

2.4. Collection of human brains

This study was approved by the Ethics Committee of the Universidad Miguel Hernández de Elche (Alicante, Spain) and was performed in accordance with the World Medical Association (WMA) Declaration of Helsinki. Brain samples (frontal cortex) were obtained from the Brain Bank at the Institute of Neuropathology, Bellvitge University Hospital (Barcelona, Spain). Cases of sporadic AD were selected on the basis of their clinical history of dementia and neuropathological CERAD diagnosis [32]. Samples were categorized according to the Braak Stage of neurofibrillary tangle pathology [33]. 12 women, 18 men; mean ± sd age, 75 ± 10 yr; Braak stage I–II, n = 10; Braak stage III–IV, n = 10; and Braak stage V–VI, n = 10, or alternatively by a rating of Aβ-phases [34]. Special care was taken not to include cases with combined pathologies to avoid bias in the pathologic series. Samples from non-demented (ND) controls (2 woman, 7 men; mean ± sd age, 53 ± 5 yr) corresponded to individuals with no clinical dementia and no evidence of brain pathology. The mean postmortem interval of the tissue was approximately 8 h for all cases, with no significant difference between groups.

2.5. Protein extraction from human brain

Frontal cortex (0.1 g) was homogenized (10% w/v) in Tris-HCl (50 mM, pH 7.4), NaCl (150 mM), Triton X-100 (0.5% w/v), Nonidet P-40 (1% w/v), and a cocktail of protease inhibitors (1:25 v/v, MilliporeSigma, Billerica, MA, USA). The homogenates were then sonicated on ice using an ultrasonic cell disruptor (Misonix, Farmingdale, NY, USA) and centrifuged for 1 h at 43,000 rpm and 4 °C. The supernatant fractions were recovered for further analyses by Western blot.

2.6. qRT-PCR analysis

RNA was extracted from human brains using the TRIzol® Reagent (Thermo Fisher Scientific, MA, USA) in the PureLink™ Micro-to-Midi Total RNA Purification System (Life Technologies, CA, USA) following the manufacturer instructions. SuperScript™ III Reverse Transcriptase (Life Technologies, CA, USA) was used to synthesize cDNAs from total RNA (2 μg) using random primers according to the manufacturer's instructions. Quantitative PCR amplification was performed on a StepOne™ Real-Time PCR System (Applied Biosystems, CA, USA). Specific TaqMan probes for human P2×2 (assay ID: Hs04176268_g1, Thermo Fisher, MA, USA) and human GAPDH were used (Applied Biosystems, CA, USA). P2×2 was quantified using the relative standard curve method normalizing it by GAPDH from the same cDNA preparation.

2.7. $A\beta_{1-40}$ peptide

Stock peptide (GenicBio, Shanghai, China) was reconstituted in DMSO to a concentration of 2.3 mM. To obtain Aβo, the peptide was aggregated in sterile H_2O (Gibco, Grand Island, NY, USA) at 80 μM using a standardized protocol (500 rpm, RT, 4 h). All treatments with Aβo were performed at a final concentration of 0.5 μM in the culture medium of mice hippocampal cells for 24 h. The presence of Aβo has been previously tested [35].

2.8. Electrophysiology

The whole-cell patch clamp technique was performed using an Axopatch 200B amplifier (AxonInstruments, CA, USA) in voltage clamp mode at a holding potential of - 60 mV. The cells were exposed to ATP (1 mM) with a perfusion system. The pipette solution was (in mM): 120 KCl, 4 $MgCl_2$, 10 HEPES, 2 ATP, 0.5 GTP, 10 BAPTA (pH 7.4, 300 mOsm). The bath solution contained (in mM): 150 NaCl, 5.4 KCl, 2 $CaCl_2$, 1 $MgCl_2$, 10 HEPES, 10 Glucose (pH 7.4, 320 mOsm) and TTX (50 nM). The analysis was performed using the Clampfit 10 software (AxonInstruments, CA, USA).

2.9. Ca^{+2} measurements

Mice hippocampal cells were loaded with the non-ratiometric Ca^{+2} sensitive fluorescent probe Fluo-4 AM (Invitrogen, CA, USA) (5 μM in DMSO) for 20 min in DPBS in standard incubation conditions. The cells were washed for 20 min with DPBS and finally washed 2 times with normal external solution, and then mounted on a Nikon TE-200-U inverted microscope (Tokyo, Japan). The cells were exposed to ATP (10 μM, 30 s) and high-potassium external solution (60 mM, 30 s) with a perfusion system. Changes in fluorescence were acquired using an iXon + EMCCD camera and analyzed with the Imaging Workbench 6.0 software (INDEC Biosystems, CA, USA).

2.10. Immunocytochemistry

Cell cultures were fixed with 4% PFA for 15 min at 4 °C, then the cells were permeabilized and blocked (0.1% Triton X-100, 10% HS) for 30 min at RT. The samples were incubated with anti-MAP1B (1:200, Santa Cruz Biotechnology, Cat# sc-8970, RRID:AB_649156, goat), anti-P2×2 (1:200, Alomone Labs Cat# APR-025, RRID:AB_2341051, rabbit), anti-APP (1:200, Abcam Cat# ab32136, RRID:AB_2289606, rabbit), anti-Fe65 (1:50, Santa Cruz Biotechnology, Cat# sc-374641, RRID:AB_10987657, mouse), anti-Rab5 (1:200, Sigma-Aldrich Cat# R7904, RRID:AB_532319, mouse) and/or anti-PGC-1α (1:200, Novus Cat# NBP1–04676, RRID:AB_1522118, rabbit) primary antibodies for 1 h at RT. Then they were incubated with the corresponding fluorescent-labeled secondary antibodies for 45 min (anti-rabbit Alexa Fluor 488, Jackson ImmunoResearch Labs Cat# 711–545–152, RRID:AB_2313584; anti-goat Cy3, Jackson ImmunoResearch Labs Cat# 305–165–003, RRID:AB_2339464; anti-goat Alexa Fluor 647, Jackson ImmunoResearch Labs Cat# 705–605–003, RRID:AB_2340436; anti-mouse Cy3, Jackson ImmunoResearch Labs Cat# 115–165–003, RRID:AB_2338680; and anti-mouse Alexa Fluor 647, Jackson ImmunoResearch Labs Cat# 715–606–151, RRID:AB_2340866). For nuclear staining, the cells were incubated with DAPI (300 nM, Tocris (Bristol, UK) for 10 min. The slides were mounted using Dako immunofluorescence mounting media (Dako, CA, USA). Images (60–63 ×) were acquired with Nikon TE-200-U inverted (Nikon, Tokyo, Japan), LSM780 NLO confocal (Zeiss, Oberkochen, Germany) and SIM ELYRA S.1 super-resolution (Zeiss, Oberkochen, Germany) microscopes. The analysis was performed using Image J (NIH, MD, USA). First, the images were deconvoluted, then for the quantification 5 different 10px x 10px ROIs were selected in each image using the marker protein in each experiment, to avoid bias in the region selection. The fluorescence intensity in these selected regions was graphed.

2.11. Immunohistochemistry

Slices were washed five times with PBS (5 min per wash) and then incubated in blocking/permeabilization solution (0.3–0.5% Triton X-100 + 10% horse serum + PBS) for 1 h. Then, slices were incubated with the primary antibodies at ice cold temperature overnight at 4 °C. Antibodies used were P2×2 (rabbit, 1:400, Alomone Labs Cat# APR-02) and MA1B (mouse, 1:400, Santa Cruz) prepared in a solution containing 0.3% Triton X-100 + 10% horse serum + PBS. Subsequently, slices were washed five times for 3 min each and incubated with the corresponding secondary antibody (conjugated with either Cy3 or AlexaFluor488) for 90 min. After incubation, nuclear staining was performed with DAPI 300 nM for 15 min. Afterwards, slices were washed five times for 3 min each and mounted with DAKO fluorescent mounting media. Images were acquired on a LSM780 NLO Zeiss confocal microscope using a 10X objective. Images were processed using both ZEN software (Carl Zeiss MicroImaging GmbH) and Image J (NIH, USA). Immunoreactivity was quantified with ImageJ using 5 regions of interest in each hippocampal area within each slice.

2.12. Western blot

Lysates from PC12 cells, mice hippocampal cultures, and human brain extracts were denatured (37ºC, 30 min), subjected to SDS-PAGE (100 V, 100 min), and transferred to nitrocellulose membranes (250 mA, 120 min). They were blocked for 2 h with 5% non-fat milk in TBS-T or Odyssey blocking buffer (Li-COR, USA). Nitrocellulose membranes were cut to incubate with the different primary antibodies: Anti-P2×2 (1:500, Alomone; 1:2000, NBP2–19655 Novus, USA), anti-Aβ (1:1000, MOAB-2, NBP2–13075 Novus, USA), anti Gβ (1:1000, Santa Cruz Biotechnology Cat# sc-378, RRID:AB_631542) and anti GAPDH (1:3000, Abcam Cat# ab9485, RRID:AB_307275) ON at 4ºC. Secondary HRP-conjugated (1:5000, Santa Cruz Biotechnology Cat# sc-2313, RRID:AB_641181, Santa Cruz Biotechnology Cat# sc-2005, RRID:AB_631736) or IRDye-conjugated (1:8000, anti-rabbit IRDye 800CW, LI-COR Biosciences Cat# 925–32213, RRID:AB_2715510 and anti-mouse IRDye 680, LI-COR Biosciences Cat# 925–68072, RRID:AB_2814912) antibodies were incubated for 1 h at RT. Immunoreactive bands were exposed using the Clarity Western ECL Substrate (Bio-Rad, CA, USA) and the Odyssey FC detection system (Li-COR, USA) or Odyssey CL× Infrared Imaging system (Li-COR, USA). Image analysis was done with the

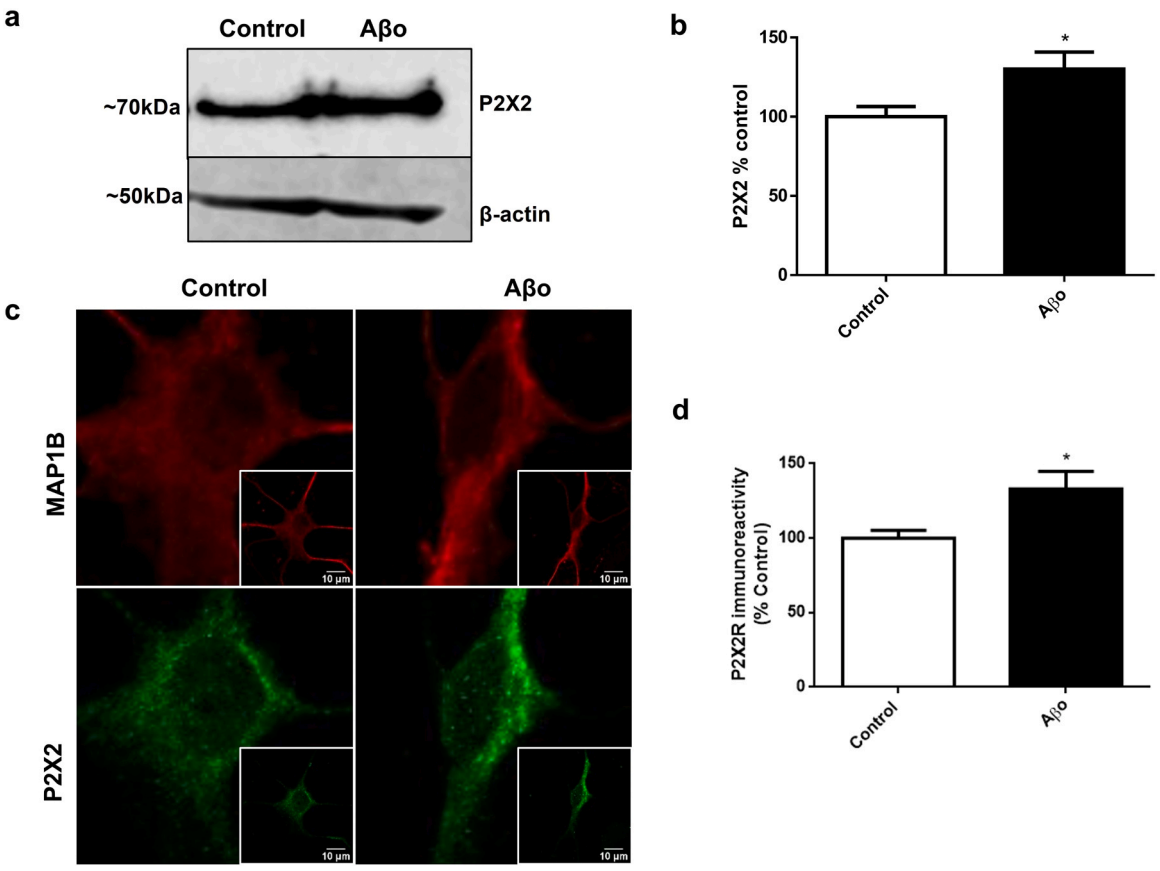

Fig. 1. P2×2 increases after Aβo treatment in mice hippocampal cells (a) Representative western blots for P2×2 and β-actin in mice hippocampal cells in control conditions and treatment with Aβo (0.5 μM, 24 h). (b) Graph shows the quantification for P2×2 normalized to β-actin and presented as percentage of control (C: 100 ± 6%, Aβo: 130 ± 11%,). All values represent mean ± SEM, n = 5, *p = 0.0328, Two-tailed *t*-test (c) Immunofluorescence for MAP1B (red) and P2×2 (green) in mice hippocampal cells in control and treatment with Aβo (0.5 μM, 24 h). (d) Graph shows the quantification for P2×2 immunoreactivity presented as percentage of control (C: 100 ± 5%, Aβo: 133 ± 12%). All values represent mean ± SEM, n = 5, *p < 0.0499, Mann-Whitney test. (For interpretation of the references to colour in this figure, the reader is referred to the web version of this article)

ImageStudio software (Image Studio Inc., WI, USA). For the correct detection and quantification of the immunoreactive bands in the experiments with overexpression, more of the control lysates was loaded in the gel. Normalization was made for each band with the corresponding loading control protein.

2.13. Experimental Design and Statistical Analysis

For treatments with Aβo mice primary hippocampal cultures were used, for overexpression of P2×2R the PC12 cell line was used. Human brain extracts were obtained from frontal cortex to evaluate P2×2 expression in patients with AD and control individuals. For immunocytochemistry samples at least three different areas were observed for each replicate. Different cells were objectively used to perform the immunorreactive analysis where random regions of interest (ROIs) were selected in each image to analyse the immunofluorescence intensity. Statistical analysis were performed in experiments with least three independent biological replicates. The only exception for this is the analysis in J20 brain slices, where we only used one animal following the principle of the 3 R. Statistical significance was determined using Student's *t*-test and one-way ANOVA for normally distributed data, or Mann-Whitney *U*-test and Kruskal-Wallis H-test for not normally distributed data. GraphPadPrism 6.0 software (GraphPad Prism (CA, USA) was used for this anlysis. n corresponds to independent replicates, and N to the number of different cells analyzed. The following results were considered statistically significant: *p < 0.05, * *p < 0.01 vs control, #p < 0.05, ##p < 0.01 vs mCherry. In graphs the data is presented as the mean ± SEM.

3. Results

3.1. The chronic treatment of hippocampal neurons with Aβo induces an increment of P2×2R

In our previous work we described that Aβo induced an increment in P2×2R expression levels in rat hippocampal neurons [26]. Now, we wanted to corroborate this observation in other cellular models such as mice hippocampal neurons, and to explore a more physiological approach such as hippocampal slices from the transgenic J20 mice. This mice expresses two mutant forms of the human APP that increases the levels of Aβ in their brains, a widely used model for AD studies [36]. To achieve this goal, we measured P2×2 protein levels in mice hippocampal cultures after a 24 h treatment with Aβo (0.5 μM, Fig. 1a). We found an increase of 30 ± 11% with respect to the control conditions (Fig. 1b, n = 5,). In parallel, we used an additional experimental approach to corroborate the observations in western blot. Using immunofluorescence and confocal microscopy we evaluated the P2×2 protein immunoreactivity (Fig. 1c), under the same experimental conditions. Quantification of the fluorescence intensity in neurons showed, in accordance with the western blot results, an increase of 33 ± 12% in P2×2 immunoreactivity after Aβo exposure compared to non-treated cells (Fig. 1d, n = 5). In another additional experimental approach, focused on provide complementary evidence about these observations, we studied the P2×2R on J20 transgenic mice. To carry out this, we used

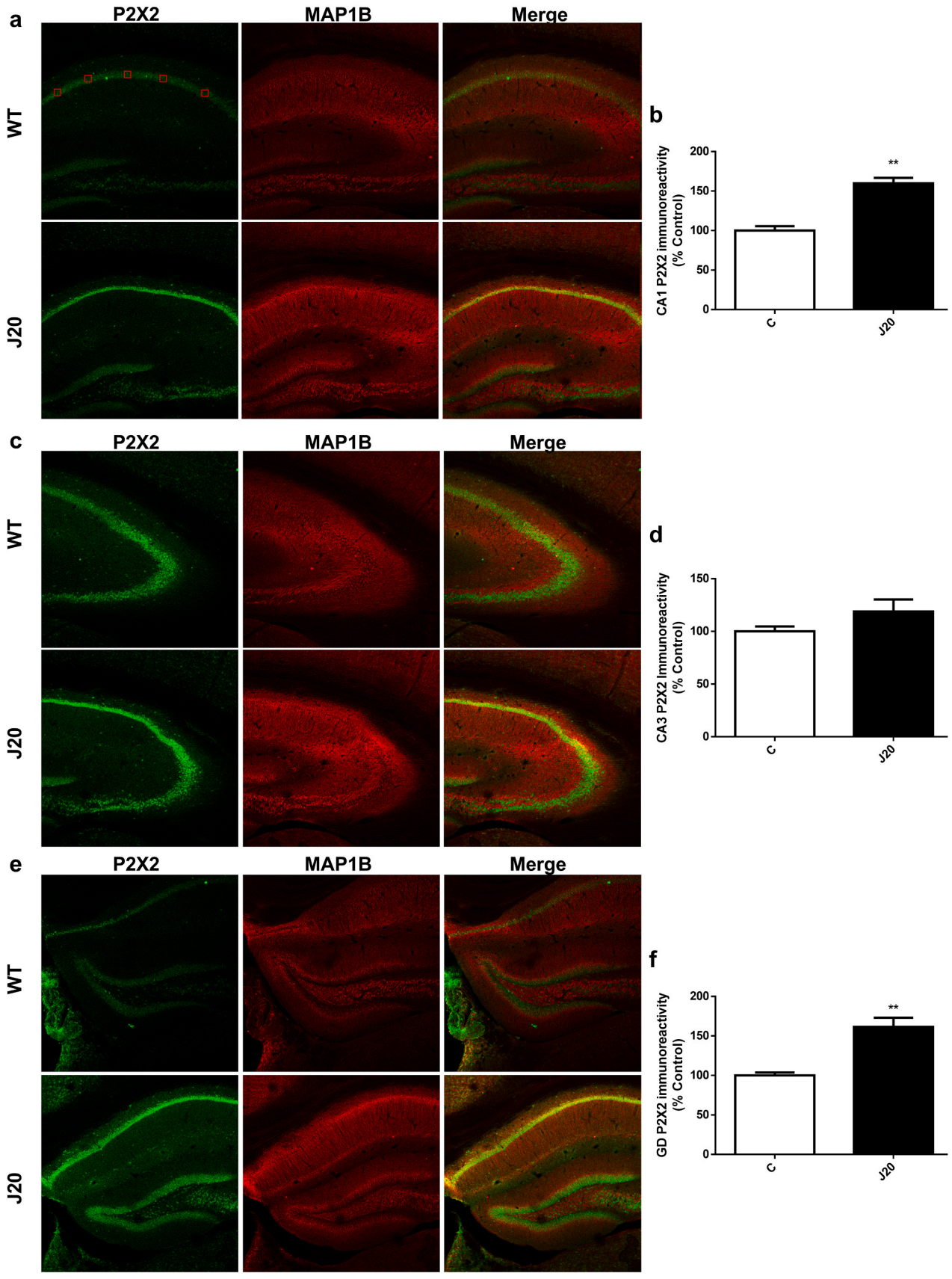

(caption on next page)

Fig. 2. Increased P2×2 immunoreactivity in hippocampus from J20 transgenic mice (a) Immunofluorescence for P2×2 (green) and MAP1B (red) in hippocampal CA1 region from WT and J20 transgenic mice. Red squares represent how the quantification was performed in these images. (b) Graph shows the quantification for P2×2 immunoreactivity in hippocampal CA1 body cells, presented as percentage of control (C: 100 ± 6%, Aβo: 160 ± 7%). All values represent mean ± SEM, N = 5, n = 1 * *p < 0.001, Mann-Whitney test. (c) Immunofluorescence for P2×2 (green) and MAP1B (red) in hippocampal CA3 region from WT and J20 transgenic mice. (d) Graph shows the quantification for P2×2 immunoreactivity in body cells presented as percentage of control (C: 100 ± 11%, Aβo: 119 ± 25%). All values represent mean ± SEM, N = 5, n = 1, ns, Mann-Whitney test. (e) Immunofluorescence for P2×2 (green) and MAP1B (red) in hippocampal Dentate Gyrus region from WT and J20 transgenic mice. (f) Graph shows the quantification for P2×2 immunoreactivity in hippocampal GD body cells, presented as percentage of control (C: 100 ± 8%, Aβo: 161 ± 26%). All values represent mean ± SEM, N = 5, n = 1 * *p < 0.001, Mann-Whitney test. (For interpretation of the references to colour in this figure, the reader is referred to the web version of this article)

hippocampal slices from a J20 transgenic mice (10 months old) and we compared the immunoreactivity of P2×2R with a WT mice (10 month) in all key areas of hippocampus (CA1 Fig. 2a, CA3 Fig. 2c, Dentate Gyrus Fig. 2e). We quantified the P2×2R immunoreactivity in the body cells of neurons in these three key areas (Fig. 2b, d and f), and we observed a significant increase in CA1 and DG of 60 ± 7% and 61 ± 26%, respectively. This important observation helps us to suggest that the Aβo toxicity could be enhancing the purinergic tone mediated by an increment on P2×2R levels. To check if these observations are important in human Aβ physiopathology, the next step was to evaluate the levels of P2×2R in brain human postmortem samples.

3.2. P2×2 expression is upregulated in the cortex of patients with Alzheimer's disease

Several studies have attempted to elucidate key elements (NMDA receptor, BDNF, GSK-3β [37–39] that could be altered in AD patients as pathognomonic signals to develop therapeutic strategies, unfortunately without success to date. Here, we evaluated the expression of P2×2R in cortex samples of patients at different stages of AD and compared the data to control samples of non-demented individuals (ND). First, we studied P2×2 protein levels through Western blot using GAPDH as a loading control (Fig. 3a, b). We observed a significant increment of 54 ± 15% in its levels in V-VI Braak stages compared to the ND controls (Fig. 3c, n = 9 (ND) and 10 (Braak Stages). We noticed that in each Braak stage group, the samples that had the higher Aβ deposition staging had the higher expression of P2×2 (0: green, A: yellow, B: orange, and C: red). Hence, we quantified P2×2 in each Aβ deposition staging-organized-sample group (Fig. 3d). The analysis showed that the C stage presented a 53 ± 14% increase compared to the ND samples (n = 9 (ND), 8 (0), 9 (A and C9 and 4 (B)). To reinforce these observations, we evaluated the P2×2 mRNA expression in the same samples. We observed a non-significant increase in the levels of P2×2 mRNA in all AD Braak stages with respect to the control samples (Fig. 3e, n = 8 (ND and I-II), 9 (III-IV) and 10 (V-VI)). Although, the samples presented a tendency to be increased according to the Aβ deposition staging. We quantified a significant increment of 132 ± 50% in the A stage compared to the ND samples (Fig. 3f, n = 8 (ND), 6 (0), 8 (A), 4 (B) and 9 (C)). These important results reinforce our hypothesis that P2×2R have a role in the physiopathology of AD. However, to consolidate this information and to demonstrate their effective contribution to Aβ toxicity, the overexpression of the receptor has to be functional.

3.3. The P2×2R overexpressed by Aβo is functional

Considering our results, one of the most important aspects to propose a role for P2×2R in this toxicity model, was to check if the increment in P2×2 after Aβo exposure was functional. To evaluate this, first we used electrophysiological patch clamp approaches. We compares the ionic conductance of ATP-evoked currents (1 mM) in control conditions and after Aβo treatment (0.5 μM, 24 h, Fig. 4a). We observed that the ATP-evoked currents in neurons exposed chronically to Aβo were significantly higher (231 ± 70%, Fig. 4b) compared to control. This indicates that the treatment overexpressed receptors (that we described in previous results) were functional, therefore these cells experiment an increment of ionic current mediated by P2×2R. To reinforce this evidence and taking into consideration that cytosolic Ca^{2+} dyshomeostasis is a central element on Aβ toxicity and P2×2R are highly permeable to Ca^{2+}, we measured intracellular calcium changes evoked by ATP (10 μM, 30 s, Fig. 4c). These experiments reported a higher Ca^{2+} cytosolic signal in Aβo treated hippocampal neurons (194 ± 24%, Fig. 4d) compared to control. To check that result was not related to a change on general cellular excitability, we used a global depolarizing experimental stimulus; high K^+ solution (60 mM, 30 s). Additionally, we used this maximal cellular response to normalize the Ca^{2+}-ATP response on treated and non-treated neurons. Both experimental conditions presented the same K^+-response (Fig. 4e). This result corroborates that the treatment with Aβo, does not affect the general excitability of the neurons and suggests that the increased response to ATP was directly related to an increase in the purinergic signaling.

3.4. Chronic treatment with Aβo decreases Fe65 nuclear/cytoplasmic ratio and PGC-1α levels in mice hippocampal neurons

After we studied P2×2R levels and function, we aimed to study Fe65 protein, a scaffold protein that interacts with both P2×2 [29] and APP [30]. First, we wanted to evaluate if the overexpressed P2×2R, induced by chronic treatment with Aβo, could induce changes in Fe65 and APP immunoreactivity. We used immunofluorescence techniques and confocal microscopy in hippocampal neurons (Fig. 5a), where we observed no changes in the Fe65 under the described experimental conditions (Fig. 5b). However, APP immunoreactivity increased by 47 ± 16% in treated hippocampal neurons (Fig. 5c). Considering that Fe65 translocates to the nucleus to activate the transcription of key genes [40], we decided to study its distribution between the nucleus (using DAPI staining) and the cytoplasm (using MAP1B immunoreactivity, Fig. 5d). As shown in the graph of Fig. 5e, the N/C ratio of Fe65 immunoreactivity decreased 28 ± 4% after chronic Aβo exposure compared to the control condition. This suggests that a reduced presence of Fe65 in the nucleus, could alter its function as a transcription regulator, compromising any reparative or corrective mechanisms to revert the Aβ insults.

One of the key proteins whose gene expression is controlled by Fe65, is PGC-1α [41], a transcriptional co-activator and a major regulator of mitochondrial biogenesis [42]. Therefore, we expected to find the total PGC-1α immunofluorescence to be affected, in correlation with previous findings. Consequently, after Aβo treatment (Fig. 5f), PGC-1α immunoreactivity decreased 15 ± 5% compared to the control mice hippocampal neurons in epifluorescence images (Fig. 5g). These results suggest that the increased P2×2R, induced by Aβo exposure, may affect the distribution of Fe65, reducing its presence in the nucleus, and causing an impact on PGC-1α levels. This could represent a set of cellular events that could be a point of "no return" in the neuron, where it is unable to support its metabolic and synaptic activity demands.

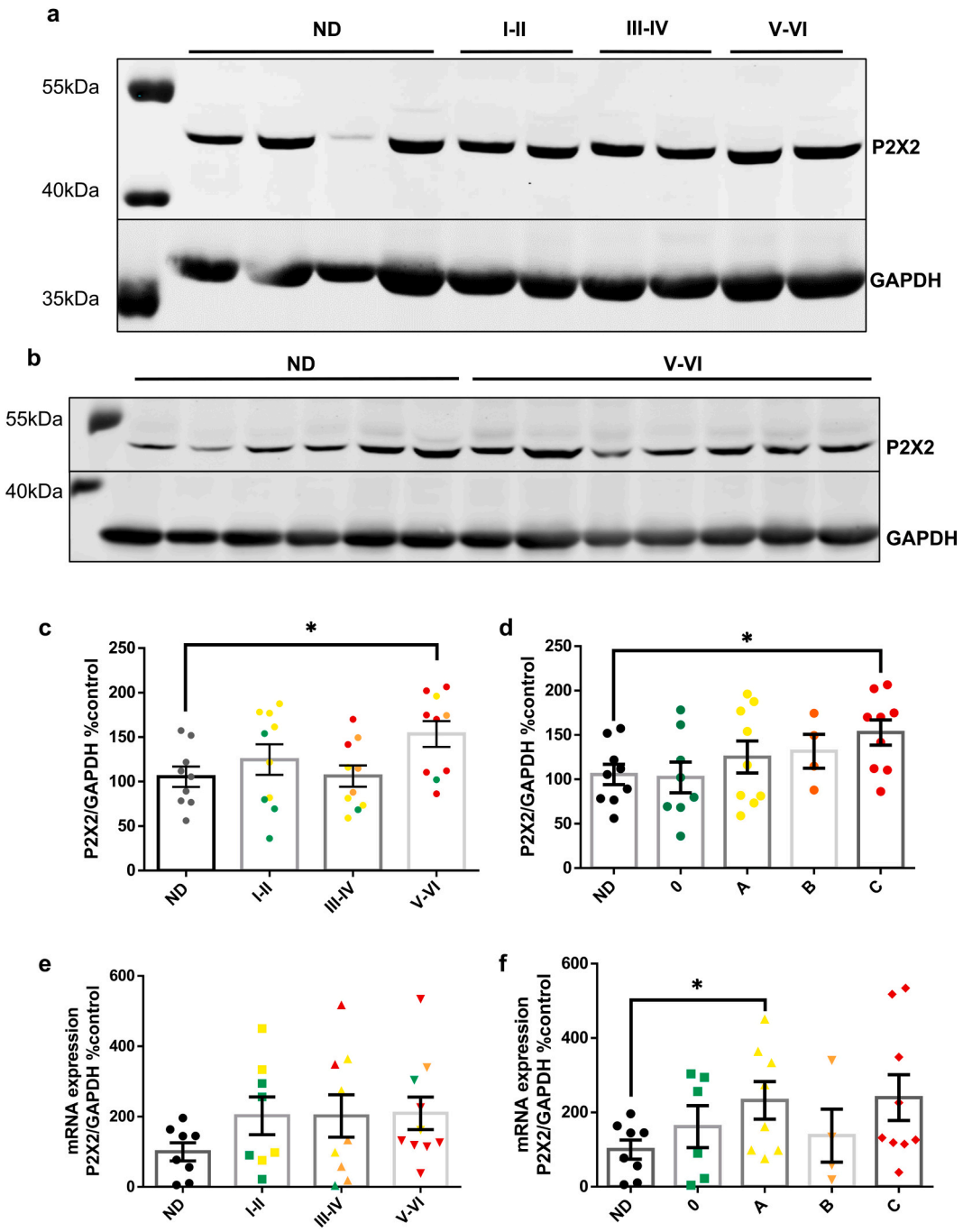

Fig. 3. Increased P2×2 expression in AD (a) Representative western blots for P2×2 and GAPDH in ND and different Braak stages of AD cortex samples. (b) Representative western blots for P2×2 and GAPDH in ND and V-VI brak stage of AD cortex samples. (c) Graph shows the quantification for P2×2 normalized to GAPDH and presented as percentage of control (ND: 106 ± 11%, I-II: 125 ± 17%, III-IV: 106 ± 12%, V-VI: 154 ± 15%). Different Aβ stages are shown by a color system 0: green, A: yellow, B: orange, C: red. All values represent mean ± SEM, n = 9 (ND) and 10 (Braak Stages), *p = 0.0202, Student's *t*-test Braak V-VI compared to ND (d) Graph shows the quantification for P2×2 in the samples at different Aβ deposition stages normalized to GAPDH and presented as percentage of control (ND: 106 ± 11%, 0: 102 ± 17%, A: 125 ± 18%, B: 132 ± 19%, C: 153 ± 14%). All values represent mean ± SEM, n = 9 (ND), 8 (0), 9 (A and C) and 4 (B), *p = 0.0194, Student's *t*-test Stage C compared to ND. (e) Graph shows the quantification for P2×2 mRNA normalized to GAPDH and presented as percentage of control (ND: 100 ± 26%, I-II: 203 ± 54%, III-IV: 202 ± 60%, V-VI: 209 ± 46%). Different Aβ stages are shown by a color system 0: green, A: yellow, B: orange, C: red. All values represent mean ± SEM, n = 8 (ND and I-II), 9 (III-IV) and 10 (V-VI), not significant p = 0.3712, one-way ANOVA. (f) Graph shows the quantification for P2×2 mRNA in the samples at different Aβ phases normalized to GAPDH and presented as percentage of control (ND: 100 ± 25%, 0: 162 ± 57%, A: 232 ± 50%, B: 138 ± 72%, C: 240 ± 61%). All values represent mean ± SEM, n = 8 (ND), 6 (0), 8 (A), 4 (B) and 9 (C) *p = 0.0348, Student's *t*-test Stage A compared to ND.

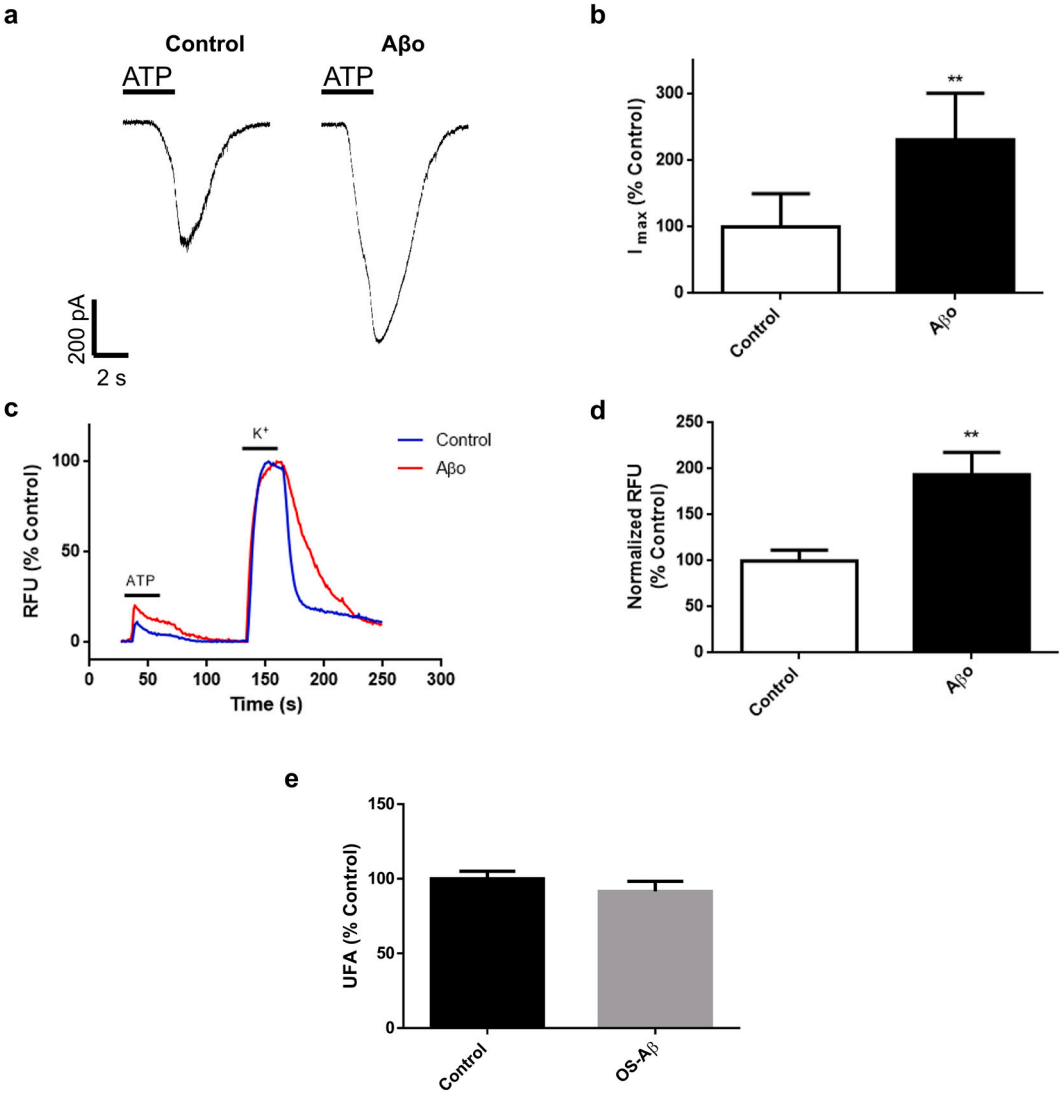

Fig. 4. ATP response increases in hippocampal neurons after Aβo exposure (a) Representative ATP (1 mM, 3 s) evoked currents in mice hippocampal cells in control and treatment with Aβo (0.5 μM, 24 h). (b) Graph shows the quantification for the I_{max} presented as percentage of control (C: 100 ± 50%, Aβo: 231 ± 70%). All values represent mean ± SEM, n = 9, * *p < 0.0078, Mann-Whitney test. (c) Representative intracellular calcium traces evoked by ATP (10 μM, 30 s) and K^+ (60 mM, 30 s) in mice hippocampal cells in control (blue) and treatment with Aβo (red, 0.5 μM, 24 h). (d) Graph shows the quantification of the fluorescence in relative units (RFU) evoked by ATP normalized to the response to K^+ and presented as percentage of control (C: 100 ± 12%, Aβo: 194 ± 94%). All values represent mean ± SEM, n = 5, * *p = 0.0037, Mann-Whitney test. (e) Graph shows the quantification of intracellular calcium changes evoked by K^+ 60 mM exposure, no significant differences were found between controls or Aβo treated neurons. (C: 100 ± 5%, Aβo: 92 ± 7%). All values represent mean ± SEM, n = 5, not significant, Mann-Whitney test.

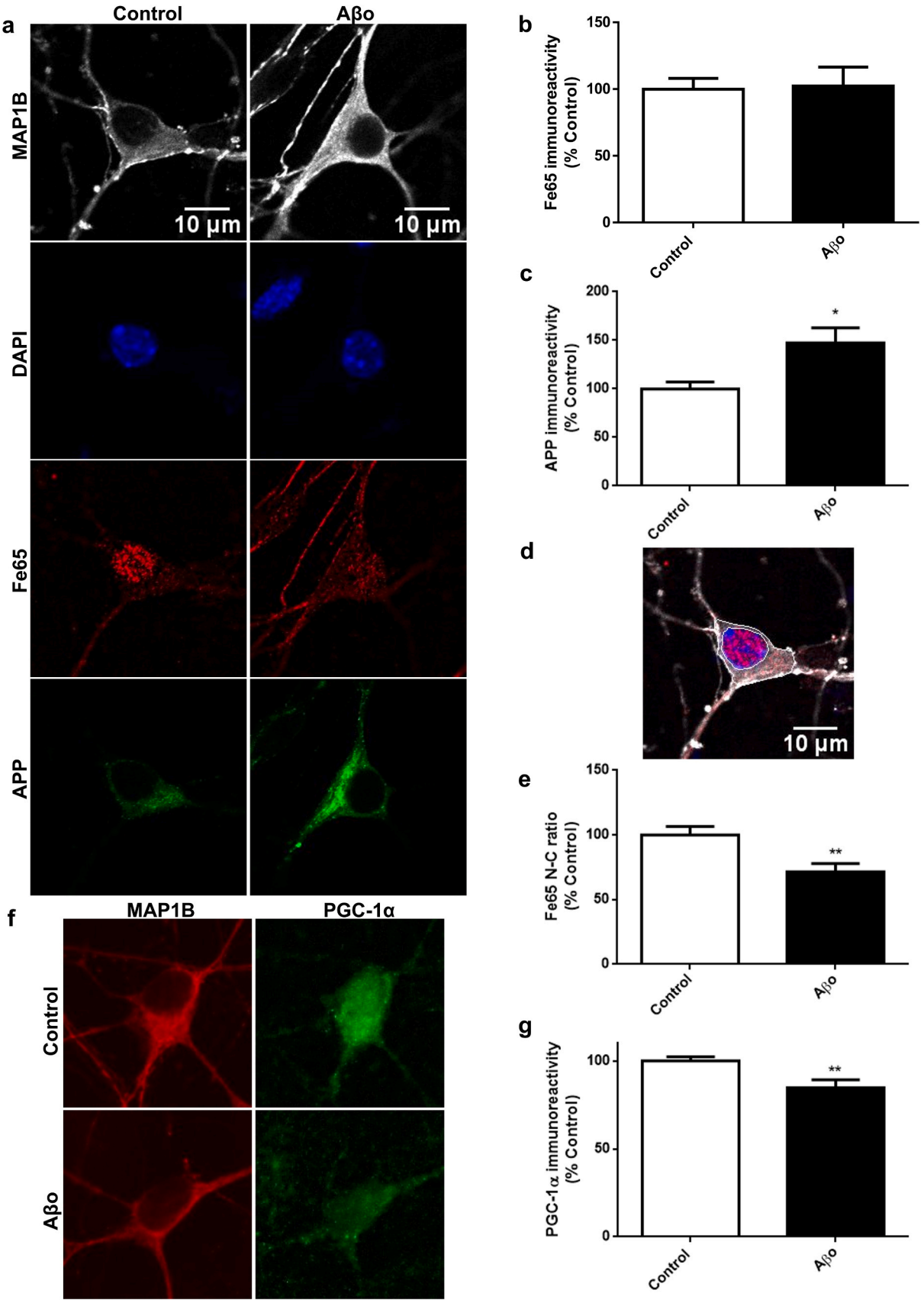

(caption on next page)

Fig. 5. Aβo treatment decreases the Fe65 nuclei/cytosolic ratio and total levels of PGC-1α (a) Immunofluorescence for MAP1B (white), Fe65 (red), APP (green), and DAPI for nuclei staining (blue) in mice hippocampal cells in control and treatment with Aβo (0.5 μM, 24 h). (b) Graph shows the quantification for Fe65 immunoreactivity presented as percentage of control (C: 100 ± 8%, Aβo: 102 ± 14%). All values represent mean ± SEM, n = 5, not significant p = 0.8878, Student's *t*-test (c) Graph shows the quantification for APP immunoreactivity presented as percentage of control (C: 100 ± 7%, Aβo: 147 ± 16%). All values represent mean ± SEM, n = 5, *p = 0.0104, Student's *t*-test (d) Schematic representation of the use of DAPI (blue) and MAP1B (white) to delimit nuclear and cytoplasmic regions for the quantification of N/C Fe65 immunoreactivity (red). (e) Graph shows the quantification for Fe65 nuclei/cytosolic ratio presented as percentage of control (C: 100 ± 7%, Aβo: 72 ± 16%). All values represent mean ± SEM, n = 5, N = 16 * *p = 0.0038, Student's *t*-test (f) Immunofluorescence for MAP1B (red) and PGC-1α (green) in mice hippocampal cells in control and treatment with Aβo (0.5 μM, 24 h). (g) Graph shows the quantification for PGC-1α immunoreactivity presented as percentage of control (C: 100 ± 2%, Aβo: 85 ± 5%). All values represent mean ± SEM, n = 5, *p < 0.005, Student's *t*-test. (For interpretation of the references to colour in this figure, the reader is referred to the web version of this article)

3.5. P2×2a overexpression induces a decrease in Fe65 nuclear/cytoplasmic ratio and in PGC1α levels

Next, we proceeded to evaluate the effect of P2×2 overexpression on Fe65 and PGC1-α immunoreactivity. To achieve this, we overexpressed either P2×2a or P2×2b in PC12 cells using cotransfection with mCherry as control. In our experiments mCherry expression after 24 h was observed mainly in the nucleus. Using immunocytochemistry (Fig. 6a), we found that P2×2 overexpression did not change Fe65 total immunoreactivity (Fig. 6b, n = 3, one-way ANOVA p = 0.5713). Then, we evaluated Fe65 distribution between the nucleus and cytoplasm using DAPI for the nuclear region and APP to select the entire cell area (Fig. 6c). Similar to treatment with Aβo, we observed a decrease of 28 ± 8% in the Fe65 immunoreactivity N/C ratio only after P2×2a transfection (n = 3, N = 12, one-way ANOVA multiple comparisons vs. Control, **p = 0.0086). After P2×2b overexpression no changes were observed (Fig. 6d, n = 3, N = 12, one-way ANOVA multiple comparions vs. mCherry, * p = 0.0166). Lastly, we studied total PGC-1α immunoreactivity in epifluorescence images in the same conditions (Fig. 6e). Again, in agreement with the results observed after Aβo treatment, the quantification of total PGC-1α immunoreactivity presented a decrease of around 34 ± 5% compared to control cells after P2×2a overexpression (n = 5, one-way ANOVA multiple comparisons vs. Control, ** p = 0.0078). No changes were observed after P2×2b overexpression (Fig. 6f, n = 5, one-way ANOVA multiple comparisons vs. Control, p = 0.6944). Interestingly, we observe that an untransfected cell (i.e. no expression of mCherry) in the surrounding area of one transfected with P2×2a, has a higher PGC1-α immunoreactivity (Fig. 6e, white arrow points to the transfected cell). Taken together, these results suggest that P2×2a exerts a more important influence on Fe65 nuclear/cytoplasmic ratio and PGC-1α levels.

3.6. Chronic treatment with Aβo promotes the endocytosis of APP by increased colocalization with Rab5

APP is a transmembrane protein that can be cleaved through the amyloidogenic pathway after its endocytosis [12]. Therefore, we aimed to evaluate the colocalization of APP with Rab5, an early endosome marker [43], as an approximation to study APP endocytosis. First, total Rab5 immunoreactivity was analyzed (Fig. 7a) and no significant differences were found compared to the control condition (Fig. 7b, n = 5, Two-tailed *t*-test, p = 0.2825). In contrast, the colocalization between APP and Rab5 increased 18 ± 16% after Aβo treatment (Fig. 7c, n = 5, N = 15, Two-tailed Mann-Whitney test, **p = 0.0027). However, this observation was not supported by the Manders coefficient analysis, since it only presented a tendency to increase after the exposure to Aβo. To perform a more robust analysis, we used super-resolution microscopy, a more resolutive technique, to evaluate the same parameters (Fig. 7d). As previously, Rab5 immunoreactivity remained unaltered (Fig. 7e, n = 5, Two-tailed Mann-Whitney test, p = 0.1298), while APP immunoreactivity increased 26 ± 10% after Aβo exposure (Fig. 7f, n = 5, Two-tailed *t*-test, *p = 0.0138). Lastly, colocalization was analyzed and a significant increment in APP-Rab5 colocalization and Manders coefficient was observed after Aβo treatment (Fig. 7g, n = 5, N = 14, Two-tailed Mann-Whitney test, ** p = 0.0069; Fig. 7h, n = 5, N = 14, Two-tailed *t*-test, ** p = 0.0075). Taken together, and using the colocalization of APP with Rab5 as a marker for endocytosis, our results suggest that Aβo promotes and increases APP endocytosis and eventually its amyloidogenic processing initiating a vicious cycle of Aβ generation.

3.7. P2×2 overexpression induces an increment in Aβ levels

Next, we wanted to evaluate if P2×2 overexpression effectively had any effect on Aβ levels. To achieve this goal, we transfected PC12 cells to overexpress P2×2a or P2×2b, and mCherry as a transfection control. The total cell lysates were analyzed using Western blot and two immunoreactive bands (around 70 and 120 kDa) corresponding to Aβ aggregates were quantified (Fig. 8a). Using this approach, we found that the overexpression of both P2×2 isoforms induced a significant increment (299 ± 55% and 300 ± 54% respectively) in Aβ levels (Fig. 8b, n = 4, Kruskal-Wallis test, vs. Control **p = 0.0020 for P2×2a, **p = 0.0050 for P2×2b; vs. mCherry ##p = 0.0035 for P2×2a, ##p = 0.0086 for P2×2b). Taken together, our results allow us to suggest that P2×2R potentiate the amyloidogenic pathway and Aβ toxicity.

4. Discussion

Several studies provide evidence that points to Aβ peptide as a key agent in the pathogenesis of AD [2], with soluble oligomers being the most toxic species [8]. Amyloidogenic processing of APP occurs mainly in endosomal compartments [9], this makes APP endocytosis a central step in the production of Aβ peptide. In parallel, ionotropic purinergic receptors are activated by ATP and it has been described that some subunits are implicated in different neurological diseases [23]. Furthermore, purinergic signaling has been described as an important feature in hippocampal neurons, particularly P2×4 and P2×2 receptors [44]. Additionally, Aβo increases the response to ATP in rat primary hippocampal cultures and PPADS, an inhibitor of P2XR, prevents several toxic features induced by Aβo [26].

In this work, we described an increase in P2×2R in mice hippocampal primary cultures after exposure to Aβo and its immunorreactivity is also increased in transgenic mice hippocampal. This result adds to the existing evidence where other P2XR have been associated with Aβ toxicity, like the increment and participation of P2×7R in microglia activation in AD [25,45]. The overexpression of P2XR could be induced by the increase of the extracellular ATP levels observed after Aβo treatments [15]. Further studies need to be carried out to validate this hypothesis. Importantly, we found that P2×2 is overexpressed in

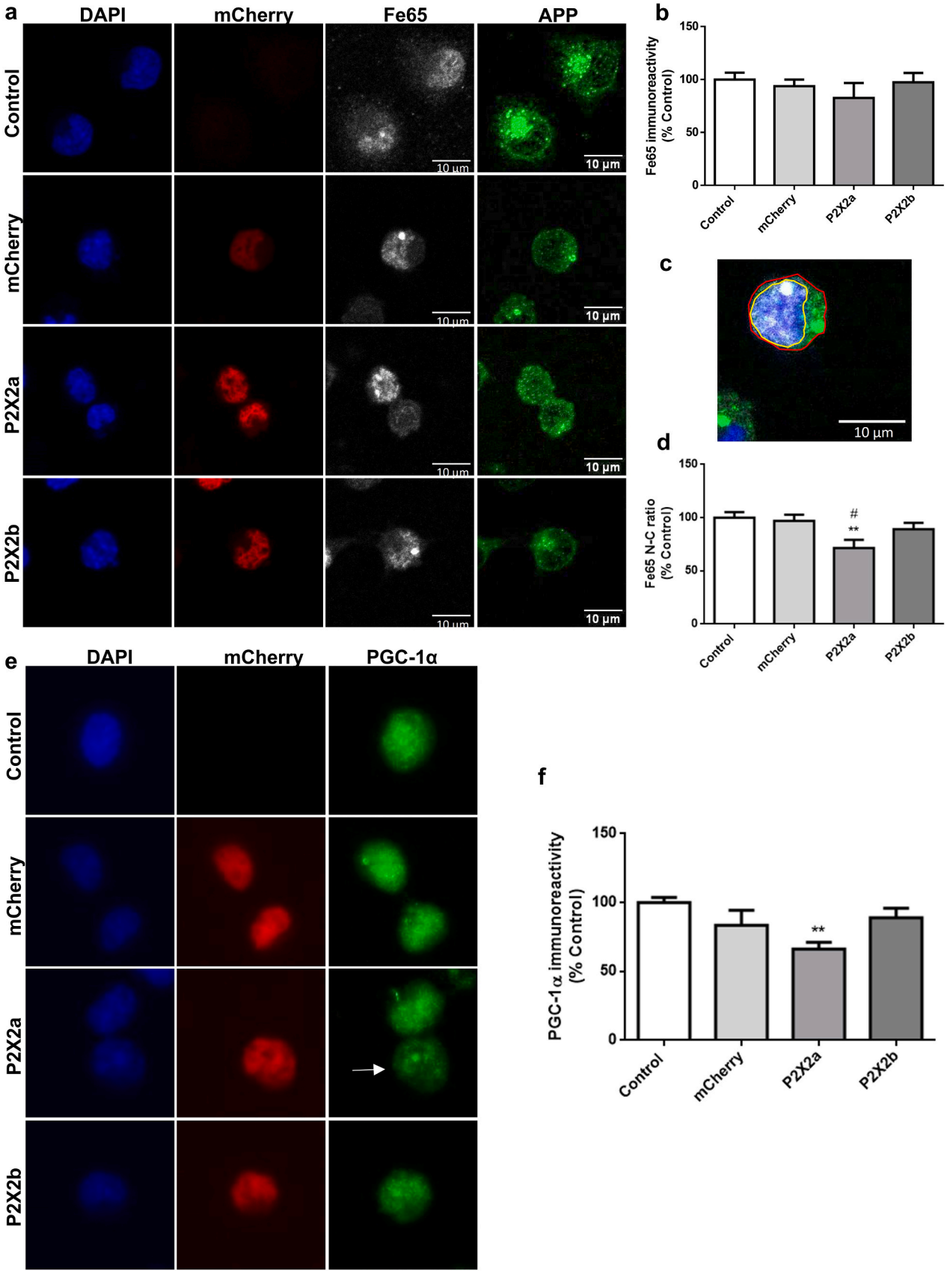

(caption on next page)

Fig. 6. P2×2a overexpression decreases Fe65 nuclei/cytosolic ratio and total levels of PGC-1α (a) Immunofluorescence for Fe65 (white), DAPI for nuclei staining (blue), and mCherry as a control for transfection in PC12 cells in control conditions and transfected with mCherry, P2×2a or P2×2b. (b) Graph shows the quantification for Fe65 immunoreactivity presented as percentage of control (C: 100 ± 6%, mCherry: 94 ± 6%, P2×2a: 83 ± 14%, P2×2b 97 ± 9%). All values represent mean ± SEM, n = 3, not significant p = 0.5713, one-way ANOVA (c) Representative picture of PC12 cell displaying DAPI (blue, framed in yellow) and APP (green, framed in red) to delimit nuclear and cytoplasmic regions for the quantification of Fe65 N/C immunoreactivity (white). (d) Graph shows the quantification for Fe65 nuclei/cytosolic ratio presented as percentage of control (C: 100 ± 5%, mCherry: 97 ± 6%, P2×2a: 72 ± 8%, P2×2b: 89 ± 6%). All values represent mean ± SEM, n = 3, N = 12, * *p = 0.0086 compared to the control, #p < 0.05 compared to mCherry, one-way ANOVA. (e) Immunofluorescence for PGC-1α (green), DAPI for nuclei staining (blue), and mCherry as a control for transfection, in PC12 cells in control conditions and transfected with mCherry, P2×2a or P2×2b. Arrow in P2×2a transfected panel indicates a cell expressing the receptor besides a non-transfected cell. (f) Graph shows the quantification for PGC-1α immunoreactivity presented as percentage of control (C: 100 ± 4%, mCherry: 83 ± 11%, P2×2a: 66 ± 5%, P2×2b: 89 ± 7%). All values represent mean ± SEM, n = 5, * *p = 0.0078 compared to the control, one-way ANOVA. (For interpretation of the references to colour in this figure, the reader is referred to the web version of this article)

human brain cortex samples of patients with AD. In these brain samples, we observed an increment in P2×2 protein (at late stages of the disease) and mRNA levels (at more early stages of the disease). In the results a dispersion of the data is observed, further analysis is needed to elucidate the reason for this dispersion, we have ruled out the sex, age and ApoE phenotype of these samples. This is the first published evidence that shows an increase in P2×2 levels in AD, since only P2×7 and P2×4 had been correlated before to this neurodegenerative disease [25]. The increment in P2×2 expression in the brain of AD subjects, together with our in vitro results, suggest that P2×2R could play a role in Aβo toxicity and AD pathogenesis.

Afterwards, we studied the effect of Aβo on APP and Fe65, an adaptor protein that interacts with P2×2a and APP [29,30]. Fe65 interacts with the intracellular domain of APP (AICD), translocates to the nucleus and participate in the transcriptional regulation of some genes [46]. One of these is the gene that codifies to PGC-1α, a master regulator of mitochondrial biogenesis [41]. Our results showed that total APP immunoreactivity is increased in hippocampal neurons after Aβ exposure, while total Fe65 immunoreactivity remained unchanged. However, we could described a reduction in the nuclear/cytoplasmic ratio of Fe65. These important observations suggest that Aβo impair Fe65 translocation to the nucleus, reducing its role as a transcription regulator factor. This is in accordance with the decrease observed in the total immunoreactivity of PGC-1α. This feature is important in the context of AD, since it has been described that mitochondrial dysfunction is a key and early hallmark in this neurodegenerative disease [47]. Several evidences point to PGC-1α as an important mediator in the impaired mitochondrial biogenesis and function observed in AD [48]. Futhermore, it has been reported a decrease in its protein and mRNA expression in AD human brain samples [49]. This decrease tightly correlates with our results and proposed mechanisms, in this work and some recent published work from our group where a downregulation of this protein was also observed in treatments with Aβ peptide [35]. Future research is necessary to determine if the decrease in the N/C ratio of Fe65 is implicated in the decrease of PGC-1α and the diminished mitochondrial biogenesis observed in AD.

In PC12 cells, APP and Fe65 total immunoreactivities are unaffected by the overexpression of P2×2a or P2×2b. On the other hand, only P2×2a induced a decrease in Fe65 N/C ratio and in total PGC-1α immunoreactivity. These results suggest that an increment in P2×2a after Aβo exposure could play a role in the described effects. Since these results were only observed after P2×2a overexpression, but not P2×2b, it can be related to the direct interaction of this isoform with Fe65 [29]. The increment of P2×2a could prevent Fe65 translocation to the nucleus by hoarding up this protein in the cytoplasm. This change could affect its capacity to regulate the transcription of important genes. On the other hand, it also suggests an increment in its availability in the cytosol to interact with other proteins, such as APP. Although conflicting evidence exists on the role of Fe65 in APP processing, recent evidence suggests that this interaction stabilizes APP, preventing its degradation through the proteasome and increasing the amyloidogenic processing [50]. Therefore, more investigation should focus on determining if the upregulation of P2×2 affects the interaction of Fe65 and APP.

We next evaluated Rab5, an early endosomal marker, and its colocalization with APP as a marker of its endocytosis. APP enters the endocytic route mainly through a clathrin-dependent pathway, and it is predominantly processed by the amyloidogenic pathway in the endosome compartments, generating the Aβ peptide [9]. Recently, it has been described that APP forms a complex with RME-6, an activator of Rab5. This mechanism regulates APP endocytosis and the transport from clathrin-coated vesicles to early endosomes [51]. In our experiments, total Rab5 immunoreactivity remained unchanged after Aβo treatment, but its colocalization with APP was significantly increased. Hence, our results suggest that Aβo favors APP endocytosis, which could potentiate its amyloidogenic processing and the production of Aβ. This result is in agreement with several previous reports where an increase in the APP amyloidogenic processing and Aβ generation have been observed after Aβo exposure [52,53]. Lastly, we observed an increment in Aβ levels after the overexpression of both P2×2 isoforms. This was an unexpected result because after all the effects observed after P2×2a, but not P2×2b overexpression, we anticipated the same for Aβ levels. This result could indicate that P2×2R function, as a cationic channel, is relevant for Aβ production. However, more in depth studies are needed to elucidate whether this mechanism is unspecific for both isoforms or the interaction of P2×2a with Fe65 plays a role in a more selective mechanism.

5. Conclusions

Together, our evidence supported an upregulation of P2×2R in AD brains that correlates tightly with our cellular and molecular evidences. These data allow us to suggest that this purinergic receptor could be involved in the pathological processes of the disease. Our in vitro results provide the first evidence and the basis for future studies to corroborate if P2×2R is part of the toxic events that increases Aβ generation, and affects Fe65 cellular distribution and PGC-1α decrease in AD. Our evidence points to P2×2R as a novel potential target that opens a new pharmacological field and provides new hope to find therapeutic alternatives to this devastating disease.

Ethics approval

Mice were treated in accordance with the regulations recommended by NIH and the Ethics Committee of the Universidad de Concepción (Concepción, Chile) complying with the current laws in Chile.

The study with human samples was approved by the Ethics Committee of the Universidad Miguel Hernández de Elche (Alicante, Spain) and was performed in accordance with the World Medical Association (WMA) Declaration of Helsinki.

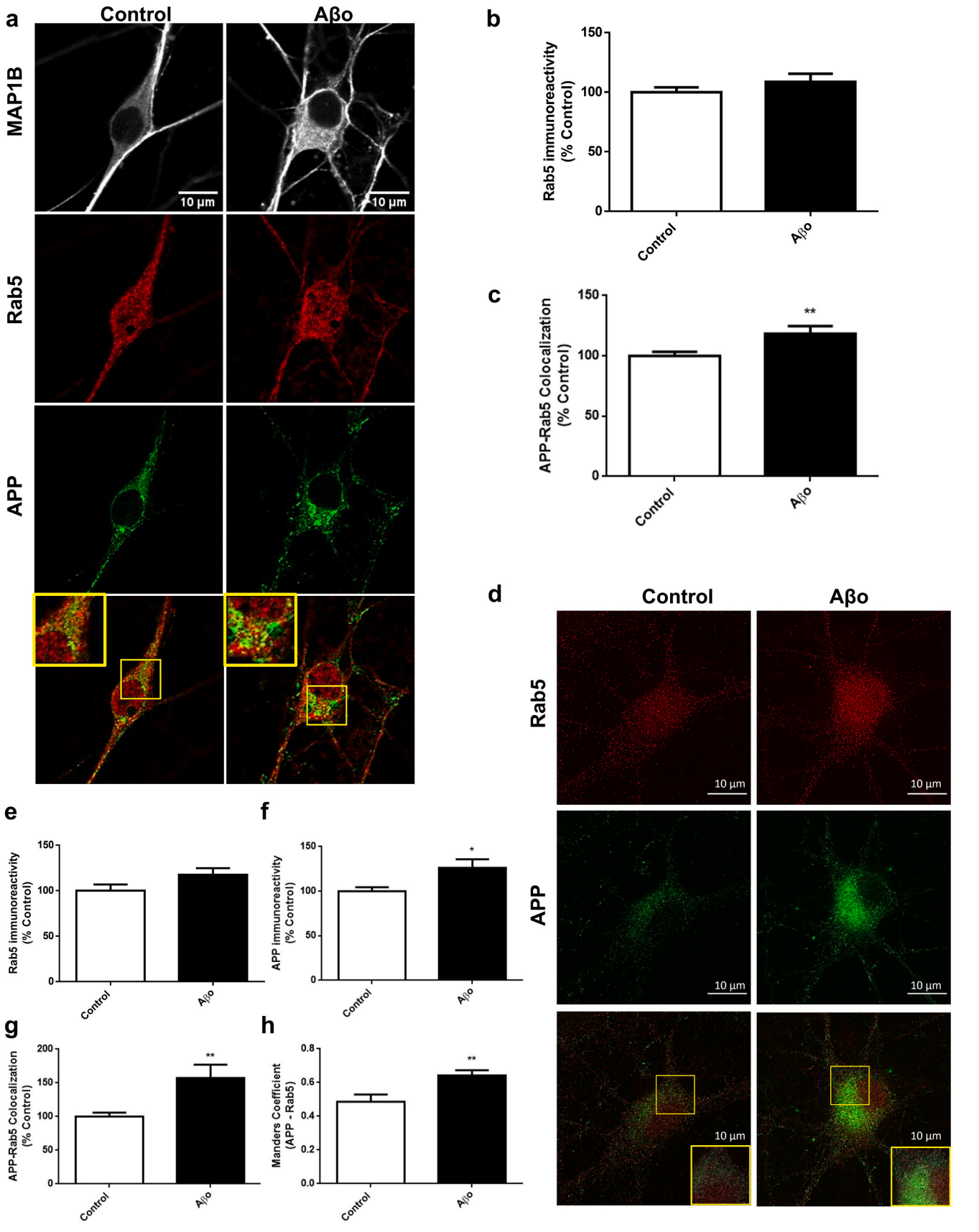

(caption on next page)

Fig. 7. Aβo increases the Rab5 and APP colocalization (a) Immunofluorescence for MAP1B (white), Rab5 (red) and APP (green) in mice hippocampal cells in control and treatment with Aβo (0.5 μM, 24 h). (b) Graph shows the quantification for Rab5 immunoreactivity presented as percentage of control (C: 100 ± 4%, Aβo: 109 ± 7%). All values represent mean ± SEM, n = 5, not significant p = 02825, Student's *t*-test (c) Graph shows the quantification for APP and Rab5 colocalization presented as percentage of control (C: 100 ± 3%, Aβo: 118 ± 6%). All values represent mean ± SEM, n = 5, N = 15, * *p = 0.0027, Mann-Whitney test (d) Superresolution immunofluorescence for Rab5 (red) and APP (green) in mice hippocampal cells in control and treatment with Aβo (0.5 μM, 24 h). (e) Graph shows the quantification for Rab5 immunoreactivity presented as percentage of control (C: 100 ± 7%, Aβo: 118 ± 7%). All values represent mean ± SEM, n = 5, not significant p = 0.1298, Mann-Whitney test (f) Graph shows the quantification for APP immunoreactivity presented as percentage of control (C: 100 ± 4%, Aβo: 126 ± 10%). All values represent mean ± SEM, n = 5, *p = 0.0138, Student's *t*-test (g) Graph shows the quantification for APP and Rab5 colocalization presented as percentage of control (C: 100 ± 6%, Aβo: 157 ± 20%). All values represent mean ± SEM, n = 5, N = 14, * *p = 0.0069, Mann-Whitney test (i) Graph shows the Manders Coefficient for APP and Rab5 (C: 0.49 ± 0.04%, Aβo: 0.64 ± 0.03%). All values represent mean ± SEM, n = 5, N = 14 * *p = 0.0075, Student's *t*-test. (For interpretation of the references to colour in this figure, the reader is referred to the web version of this article)

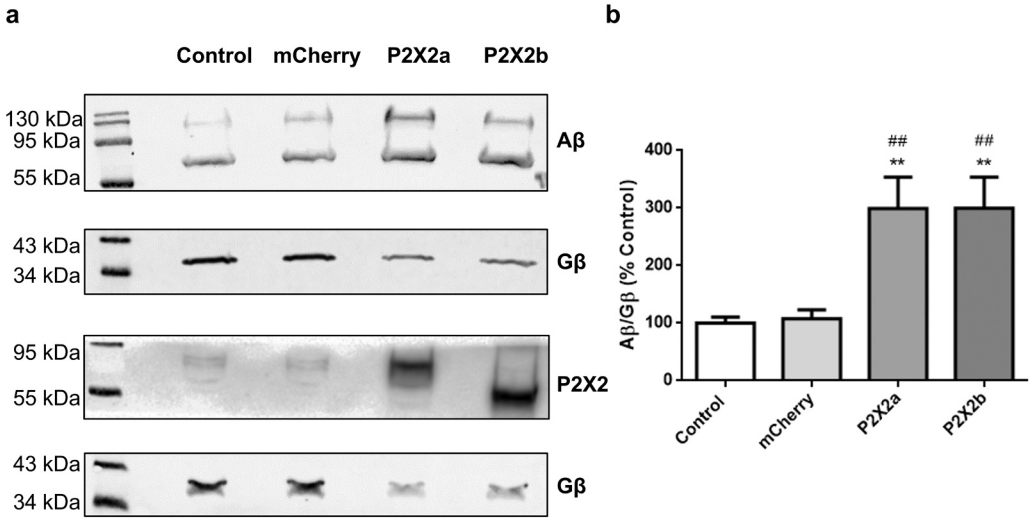

Fig. 8. P2×2 overexpression increases Aβ levels (a) Representative western blots for Aβ, P2×2, and Gβ (subunit from G protein) used to normalize, in PC12 cells in control conditions and transfected with mCherry, P2×2a, or P2×2b. Note that more lysates from the control cells (control and mCherry) was used to detect the immunoreactive bands. (b) Graph shows the quantification for Aβ normalized to Gβ and presented as percentage of control (C: 100 ± 11%, mCherry: 108 ± 15%, P2×2a: 299 ± 55%, P2×2b: 300 ± 54%). All values represent mean ± SEM, n = 4, * *p = 0.0020 for P2×2a and * *p = 0.0050 for P2×2b comparing to control, ##p = 0.0035 for P2×2a and ##p = 0.0086 for P2×2b comparing to mCherry, Kruskal-Wallis test.

CRediT authorship contribution statement

PG, DM, JS and JF contributed to the study conception and design. Material preparation and data collection were performed by DM, PG, IC, OR, JP, TS and PC. Data analysis was performed by DM, PG and IC. The manuscript was written by PG and JF, all authors make their contributions to the actual version of the manuscript. All authors read and approved the final manuscript.

Conflict of interest statement

None

Acknowledgments

This work was supported by the FONDECYT [grant numbers 1161078, 1200908 (JF)], and by the Instituto de Salud Carlos III [grant numbers PI15/00665, PI19-01359] (co-financed by the Fondo Europeo de Desarrollo Regional, "Investing in your future") (JSV). PAG is a PhD student of CONICYT [grant number 21160392]. We thank Laurie Aguayo for editing this manuscript, Ixia Cid for her technical assistance, and CMA-BIOBIO for their technical support.

References

[1] A. Serrano-Pozo, M.P. Frosch, E. Masliah, B.T. Hyman, Neuropathological alterations in Alzheimer disease, Cold Spring Harb. Perspect. Med. 1 (1) (2011), 006189.
[2] A. Mudher, S. Lovestone, Alzheimer's disease-do tauists and baptists finally shake hands? TRENDS Neurosci. 25 (2002) 22–26.
[3] J. Fuentealba, A. Dibarrart, F. Saez-Orellana, M.C. Fuentes-Fuentes, C.N. Oyanedel, J. Guzmán, C. Perez, J. Becerra, L.G. Aguayo, Synaptic silencing and plasma membrane dyshomeostasis induced by amyloid-beta peptide are prevented by Aristotelia chilensis enriched extract, J. Alzheimers Dis. 31 (4) (2012) 879–889.
[4] J. Parodi, F.J. Sepúlveda, J. Roa, C. Opazo, N.C. Inestrosa, L.G. Aguayo, β-amyloid causes depletion of synaptic vesicles leading to neurotransmission failure, J. Biol. Chem. 285 (4) (2010) 2506–2514.
[5] F.J. Sepulveda, J. Parodi, R.W. Peoples, C. Opazo, L.G. Aguayo, Synaptotoxicity of Alzheimer beta amyloid can be explained by its membrane perforating property, PloS One 5 (7) (2010) 11820.
[6] G.A. Krafft, W.L. Klein, ADDLs and the signaling web that leads to Alzheimer's disease, Neuropharmacology 59 (4–5) (2010) 230–242.
[7] F. Sáez-Orellana, P.A. Godoy, C.Y. Bastidas, T. Silva-Grecchi, L. Guzmán, L. G. Aguayo, J. Fuentealba, ATP leakage induces P2XR activation and contributes to acute synaptic excitotoxicity induced by soluble oligomers of beta-amyloid peptide in hippocampal neurons, Neuropharmacology 100 (2016) 116–123.
[8] B. Mroczko, M. Groblewska, A. Litman-Zawadzka, J. Kornhuber, P. Lewczuk, Amyloid β oligomers (AβOs) in Alzheimer's disease, J. Neural Transm. 125 (2) (2018) 177–191.
[9] G. Thinakaran, E.H. Koo, Amyloid precursor protein trafficking, processing, and function, J. Biol. Chem. 283 (44) (2008) 29615–29619.
[10] U.C. Müller, T. Deller, M. Korte, Not just amyloid: physiological functions of the amyloid precursor protein family, Nat. Rev. Neurosci. 18 (5) (2017) 281–298.
[11] S. Parvathy, I. Hussain, E.H. Karran, A.J. Turner, N.M. Hooper, Cleavage of Alzheimer's amyloid precursor protein by α-secretase occurs at the surface of neuronal cells, Biochemistry 38 (30) (1999) 9728–9734.
[12] E.H. Koo, S.L. Squazzo, Evidence that production and release of amyloid beta-protein involves the endocytic pathway, J. Biol. Chem. 269 (26) (1994) 17386–17389.
[13] O.M. Grbovic, P.M. Mathews, Y. Jiang, S.D. Schmidt, R. Dinakar, N.B. Summers-Terio, B.P. Ceresa, R.A. Nixon, A.M. Cataldo, Rab5-stimulated Up-regulation of the Endocytic Pathway Increases Intracellular β-Cleaved Amyloid Precursor Protein Carboxyl-terminal Fragment Levels and Aβ Production, J. Biol. Chem. 278 (2003) 31261–31268.
[14] N. Arispe, E. Rojas, H.B. Pollard, Alzheimer disease amyloid beta protein forms calcium channels in bilayer membranes: blockade by tromethamine and aluminum, Proc. Natl. Acad. Sci. U.S.A. 90 (2) (1993) 567–571.
[15] J. Fuentealba, A.J. Dibarrart, M.C. Fuentes-Fuentes, F. Saez-Orellana, K. Quiñones, L. Guzmán, C. Perez, J. Becerra, L.G. Aguayo, Synaptic failure and adenosine triphosphate imbalance induced by amyloid-beta aggregates are prevented by blueberry-enriched polyphenols extract, J. Neurosci. Res 89 (9) (2011) 1499–1508.
[16] M.J. Calkins, M. Manczak, P. Mao, U. Shirendeb, P.H. Reddy, Impaired mitochondrial biogenesis, defective axonal transport of mitochondria, abnormal mitochondrial dynamics and synaptic degeneration in a mouse model of Alzheimer's disease, Hum. Mol. Genet. 20 (23) (2011) 4515–4529.

[17] S.Y. Kim, J.H. Moon, H.G. Lee, S.U. Kim, Y.B. Lee, ATP released from beta-amyloid-stimulated microglia induces reactive oxygen species production in an autocrine fashion, Exp. Mol. Med. 39 (6) (2007) 820–827.

[18] M.P. Mattson, B. Cheng, D. Davis, K. Bryant, I. Lieberburg, R.E. Rydel, beta-Amyloid peptides destabilize calcium homeostasis and render human cortical neurons vulnerable to excitotoxicity, J. Neurosci. 12 (2) (1992) 376–389.

[19] W. Lee, H. Yin, Y. Shen, The mechanisms of neuronal death produced by mitochondrial toxin 3-nitropropionic acid: the roles of N-methyl-D-aspartate glutamate receptors and mitochondrial calcium overload, Neuroscience 112 (3) (2002) 707–716.

[20] G. Burnstock, P2X ion channel receptors and inflammation, Purinergic Signal. 12 (1) (2016) 59–67.

[21] B.S. Khakh, D. Gittermann, D.A. Cockayne, A. Jones, ATP modulation of excitatory synapses onto interneurons, J. Neurosci. 23 (19) (2003) 7426–7437.

[22] B.S. Khakh, R.A. North, Neuromodulation by extracellular ATP and P2X receptors in the CNS, Neuron 76 (1) (2012) 51–69.

[23] F. Sáez-Orellana, P.A. Godoy, T. Silva-Grecchi, K.M. Barra, J. Fuentealba, Modulation of the neuronal network activity by P2X receptors and their involvement in neurological disorders, Pharmacol. Res. 101 (2015) 109–115.

[24] Y.-J. Lee, S.B. Han, S.Y. Nam, K.W. Oh, J.T. Hong, Inflammation and Alzheimer's disease, Arch. Pharmacal Res. 33 (10) (2010) 1539–1556.

[25] P.A. Godoy, O. Ramírez-Molina, J. Fuentealba, Exploring the role of P2X receptors in Alzheimer's disease, Front. Pharmacol. 10 (1330) (2019).

[26] F. Sáez-Orellana, M.C. Fuentes-Fuentes, P.A. Godoy, T. Silva-Grecchi, J.D. Panes, L. Guzmán, G.E. Yévenes, J. Gavilán, T.M. Egan, L.G. Aguayo, J. Fuentealba, P2X receptor overexpression induced by soluble oligomers of amyloid beta peptide potentiates synaptic failure and neuronal dyshomeostasis in cellular models of Alzheimer's disease, Neuropharmacology 128 (2018) 366–378.

[27] K. Kaczmarek-Hájek, E. Lörinczi, R. Hausmann, A. Nicke, Molecular and functional properties of P2X receptors—recent progress and persisting challenges, Purinergic Signal. 8 (3) (2012) 375–417.

[28] R.A. North, Molecular physiology of P2X receptors, Physiol. Rev. 82 (4) (2002) 1013–1067.

[29] M. Masin, D. Kerschensteiner, K. Dümke, M.E. Rubio, F. Soto, Fe65 interacts with P2×2 subunits at excitatory synapses and modulates receptor function, J. Biol. Chem. 281 (7) (2006) 4100–4108.

[30] S.L. Sabo, L.M. Lanier, A.F. Ikin, O. Khorkova, S. Sahasrabudhe, P. Greengard, J. D. Buxbaum, Regulation of β-amyloid secretion by FE65, an amyloid protein precursor-binding protein, J. Biol. Chem. 274 (12) (1999) 7952–7957.

[31] J. Gavilan, D. Mennickent, O. Ramirez-Molina, S. Triviño, C. Perez, T. Silva-Grecchi, P.A. Godoy, J. Becerra, L.G. Aguayo, G. Moraga-Cid, V.S. Martin, G. E. Yevenes, P.A. Castro, L. Guzman, J. Fuentealba, 17 oxo sparteine and lupanine, obtained from cytisus scoparius, exert a neuroprotection against soluble oligomers of amyloid-β toxicity by nicotinic acetylcholine receptors, J. Alzheimer'S. Dis. 67 (1) (2019) 343–356.

[32] S.S. Mirra, M. Gearing, Jr McKeel DW, B.J. Crain, J.P. Hughes, G. van Belle, A. Heyman, Interlaboratory comparison of neuropathology assessments in Alzheimer's disease: a study of the Consortium to Establish a Registry for Alzheimer's Disease (CERAD), J. Neuropathol. Exp. Neurol. 53 (3) (1994) 303–315.

[33] H. Braak, E. Braak, Neuropathological stageing of Alzheimer-related changes, Acta Neuropathol. 82 (4) (1991) 239–259.

[34] I. Alafuzoff, D.R. Thal, T. Arzberger, N. Bogdanovic, S. Al-Sarraj, I. Bodi, S. Boluda, O. Bugiani, C. Duyckaerts, E. Gelpi, S. Gentleman, G. Giaccone, M. Graeber, T. Hortobagyi, R. Höftberger, P. Ince, J.W. Ironside, N. Kavantzas, A. King, P. Korkolopoulou, G.G. Kovács, D. Meyronet, C. Monoranu, T. Nilsson, P. Parchi, E. Patsouris, M. Pikkarainen, T. Revesz, A. Rozemuller, D. Seilhean, W. Schulz-Schaeffer, N. Streichenberger, S.B. Wharton, H. Kretzschmar, Assessment of β-amyloid deposits in human brain: a study of the BrainNet Europe Consortium, Acta Neuropathol. 117 (3) (2009) 309–320.

[35] J.D. Panes, P.A. Godoy, T. Silva-Grecchi, M.T. Celis, O. Ramirez-Molina, J. Gavilan, C. Muñoz-Montecino, P.A. Castro, G. Moraga-Cid, G.E. Yévenes, L. Guzmán, J. L. Salisbury, E. Trushina, J. Fuentealba, Changes in PGC-1α/SIRT1 signaling impact on mitochondrial homeostasis in amyloid-beta peptide toxicity model, Front. Pharmacol. 11 (2020) 709.

[36] T. Karl, S. Bhatia, D. Cheng, W.S. Kim, B. Garner, Cognitive phenotyping of amyloid precursor protein transgenic J20 mice, Behav. Brain Res. 228 (2) (2012) 392–397.

[37] H. Bi, C.-I. Sze, N-methyl-D-aspartate receptor subunit NR2A and NR2B messenger RNA levels are altered in the hippocampus and entorhinal cortex in Alzheimer's disease, J. Neurol. Sci. 200 (1–2) (2002) 11–18.

[38] R.M. Holsinger, J. Schnarr, P. Henry, V.T. Castelo, M. Fahnestock, Quantitation of BDNF mRNA in human parietal cortex by competitive reverse transcription-polymerase chain reaction: decreased levels in Alzheimer's disease, Mol. Brain Res. 76 (2) (2000) 347–354.

[39] J.-J. Pei, E. Braak, H. Braak, I. Grundke-Iqbal, K. Iqbal, B. Winblad, R.F. Cowburn, Distribution of active glycogen synthase kinase 3β (GSK-3β) in brains staged for Alzheimer disease neurofibrillary changes, J. Neuropathol. Exp. Neurol. 58 (9) (1999) 1010–1019.

[40] X. Cao, T.C. Südhof, A transcriptively active complex of APP with Fe65 and histone acetyltransferase Tip60, Science 293 (5527) (2001) 115–120.

[41] A. Robinson, S. Grösgen, J. Mett, V.C. Zimmer, V.J. Haupenthal, B. Hundsdörfer, C. P. Stahlmann, Y. Slobodskoy, U.C. Müller, T. Hartmann, R. Stein, M.O. Grimm, Upregulation of PGC-1α expression by A lzheimer's disease-associated pathway: presenilin 1/amyloid precursor protein (APP)/intracellular domain of APP, Aging Cell 13 (2) (2014) 263–272.

[42] M.B. Hock, A. Kralli, Transcriptional control of mitochondrial biogenesis and function, Annu. Rev. Physiol. 71 (2009) 177–203.

[43] J.-P. Gorvel, P. Chavrier, M. Zerial, J. Gruenberg, rab5 controls early endosome fusion in vitro, Cell 64 (5) (1991) 915–925.

[44] P. Agostinho, D. Madeira, L. Dias, A.P. Simões, R.A. Cunha, P.M. Canas, Purinergic signaling orchestrating neuron-glia communication, Pharmacol. Res. 162 (2020), 105253.

[45] P. Suresh, S. Phasuk, I.Y. Liu, Modulation of microglia activation and Alzheimer's disease: CX3 chemokine ligand 1/CX3CR and P2×7R signaling, Tzu Chi Med. J. 33 (1) (2021) 1–6.

[46] E. Buoso, C. Lanni, G. Schettini, S. Govoni, M. Racchi, β-Amyloid precursor protein metabolism: focus on the functions and degradation of its intracellular domain, Pharmacol. Res. 62 (4) (2010) 308–317.

[47] X. Wang, W. Wang, L. Li, G. Perry, H.G. Lee, X. Zhu, Oxidative stress and mitochondrial dysfunction in Alzheimer's disease, Biochim. Biophys. Acta 1842 (8) (2014) 1240–1247.

[48] G. Sweeney, J. Song, The association between PGC-1α and Alzheimer's disease, Anat. Cell Biol. 49 (1) (2016) 1–6.

[49] W. Qin, V. Haroutunian, P. Katsel, C.P. Cardozo, L. Ho, J.D. Buxbaum, G. M. Pasinetti, PGC-1α expression decreases in the Alzheimer disease brain as a function of dementia, Arch. Neurol. 66 (3) (2009) 352–361.

[50] K.F. Lau, W.N. Chow, J. Ngo, Y.W. Chen, V. Tam, E. Chan, C. Miller, FE65 serine-610 phosphorylation and its functional implications in Alzheimer disease amyloid precursor protein processing, Hong. Kong Med. J. 25 Suppl 7 (5 Supplement 7) (2019) 44–47.

[51] S. Eggert, T. Gruebl, R. Rajender, C. Rupp, B. Sander, A. Heesch, M. Zimmermann, S. Hoepfner, H. Zentgraf, S. Kins, The Rab5 activator RME-6 is required for amyloid precursor protein endocytosis depending on the YTSI motif, Cell. Mol. Life Sci. 77 (2020) 5223–5242.

[52] M. Rolland, R. Powell, M. Jacquier-Sarlin, S. Boisseau, R. Reynaud-Dulaurier, J. Martinez-Hernandez, L. André, E. Borel, A. Buisson, F. Lanté, Effect of Aβ oligomers on neuronal APP triggers a vicious cycle leading to the propagation of synaptic plasticity alterations to healthy neurons, J. Neurosci.: Off. J. Soc. Neurosci. 40 (2020) 5161–5176.

[53] D. Tampellini, N. Rahman, E.F. Gallo, Z. Huang, M. Dumont, E. Capetillo-Zarate, T. Ma, R. Zheng, B. Lu, D.M. Nanus, M.T. Lin, G.K. Gouras, Synaptic activity reduces intraneuronal Aβ, promotes APP transport to synapses, and protects against Aβ-related synaptic alterations, J. Neurosci. 29 (31) (2009) 9704–9713.